Analysis and Modeling of Human – Seat Interaction Using Bio and Contact Mechanics

Yuezhi (Sean) LIU, Jiancheng JI, Xianzhi ZHONG and Jeff XI

Department of Aerospace Engineering, Ryerson University

Abstract Presented in this paper is a method to study the interaction between human body and aircraft seat for the comfortability analysis. First, the human body is modeled using the bio mechanics and divided into a number of body segments connected by joints according to human anatomy. The angles between each body segments are obtained from mathematical analysis from existing bio mechanical research data. The contact forces between human body and the seat are modeled using pairs of bi-lateral point forces. These forces are calculated and located with the analysis of the center of gravity of each body segments and average muscular structure of the human body. The geometry of the human body is derived from the spine curves of the sitting position and average body type. Second, the pressure distribution between the human body and the seat is modeled and calculated using the contact stress theory. The results of the two parts are combined to analyze the comfortability in relation to different posture and backrest recline angles. At the end, the modeling result is compared with pressure sensor data for validation.

Keywords: Bio-modeling, contact modeling, seat-human interaction, seating comfort

1 Introduction

Aircraft passengers' comfort has become an increasing concern for airliners as it greatly affects passenger's travel experience [1]. In recent years, the study of comfortability for cabin environment has been one of the most important topics in this research. The existing studies so far contain measurement and analysis of human muscle activity [2], geometric parameters of seat [3], postural analysis [4-6], with the pressure distribution between the human body and seat identified as the key in the evaluation of sitting comfort [7]. Ideally, the pressure distribution between the human body and seat should be homogeneous, but very often there exist some high pressure areas causing discomfort [8]. The past studies include static and dynamic pressure, with the former being directly associated with comfort ratings [9]. The latter was used to evaluate the human postural change in order to adjust the posture and

reduce the discomfort [8,10,11]. Some software, such as AnyBody, OpenSim, PAM-comfort and Adams, has been used to develop human bio-models for seating comfort research [12,13]. These studies are used to calculate the interface pressure and surface friction forces [14]. However, most researches assume the spine as one segment with no consideration of the influence of the spine curve.

The objective of this study is to develop a complete bio-model for sitting comfort through the following steps: 1) put forward a method to model a spine curve in relation to the human contact points with the seat; 2) apply a multi-body dynamics method to model the human forces at the contact points; 3) apply a contact mechanics method to model the contact pressure distribution; 4) validate the proposed model by the experiment.

2 Modeling

2.1 System Description

Fig. 1 illustrates a person sitting in a seat with contact forces at contact points. The human body is divided into nine segments: feet, calf, thigh, pelvis, lumbar, thoracic-2, thoracic-1, cervical and head. For modeling, a global coordinate system O_XYZ is set with the origin at a point in space. $o_0\_x_0y_0z_0$ is the local coordinate system attached to the seat, and $o_i\_x_iy_iz_i$ is a body segment coordinate system. Symbol m_i represents the mass of ith segment, g is the gravitational constant, l_i represents the length of ith segment, θ_i represents the angle of ith segment joint, $\mathbf{w}_i = [\mathbf{f}_i \quad \mathbf{m}_i]^T$ is the wrench of ith segment including force vector $\mathbf{f}_i$ and moment vector $\mathbf{m}_i$. The force vector is decomposed to the normal f_{ni} and tangential force f_{ti}. φ is the recline angle of the seat which is defined between 90-180 degree.

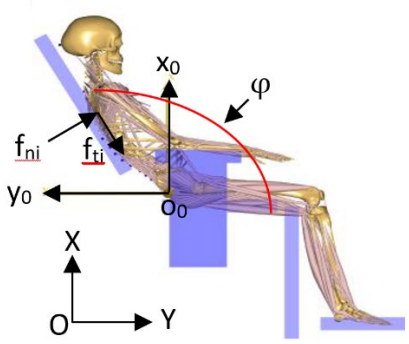

Fig. 1. Human sits on the seat

If a person sits upright, the body weight is mainly supported by the hip and thighs. Once the human leans against the backrest especially when the seat reclines, it will generate the contact forces between the human and the backrest. The first part of this method to model the spine curve in different sitting postures and obtain the joint angles and contact points, based on which the contact forces and pressure distributions can be determined.

2.2 Modeling of Spine Curve

The human spine is modeled by curve fitting the existing bio mechanical research data [15]. The following equations are obtained for different common seating postures. The erected posture is modeled as

$$f_E = -1.525 \times 10^{-10}x^7 + 6.114 \times 10^{-8}x^6 - 9.939 \times 10^{-6}x^5 + 8.389 \times 10^{-4}x^4 - 0.03894x^3 + 0.9667x^2 -$$

$$11.37x + 41.57 \quad (1)$$

The normal posture is modeled as

$$f_N = 1.753e^{-10}x^7 - 4.755e^{-8}x^6 + 4.97e^{-6}x^5 - 0.0002511x^4 + 0.006453x^3 - 0.09109x^2 + 1.072x - 16.78 \quad (2)$$

The slouched posture is modeled as

$$f_S = 1.39 \times 10^{-10}x^7 - 3.5 \times 10^{-8}x^6 + 3.214 \times 10^{-6}x^5 - 1.233 \times 10^{-4}x^4 + 1.329 \times 10^{-3}x^3 + 0.02428x^2 - 0.3235x - 10.13 \quad (3)$$

where $x \in [15, 75]\text{cm}$ represents the spine by connecting the pelvis to the head. For used polynomials, the reason for a particular degree chosen is that the curvature of the curve near the end points of the data doesn't change sharply. It is especially important in this case as those equations are used to calculate the instantaneous radius. The orientation of this base line is related to the recline angle of the seat. The given spine range can be scaled up or down to account for the height difference of individuals.

For force analysis, a spine is segmented according to the position percentage of spine segments: cervical, thoracic-1, thoracic-2 and lumbar. These segments are linearized and connected by lines through the nodal points modeled as revolute joints. Since the length of each segment is known, its coordinate can be determined by

$$L = \int_b^a \sqrt{1 + \left(\frac{df}{dx}\right)^2}\, dx \quad (4)$$

where a and b are the x coordinates of the two end points of each segment. By using our proposed method, the linearized spine model can be determined for the three postures as shown in Fig. 2. The relative angles between adjacent lines are determined to represent the joint angles as listed in Table 1 for the three postures.

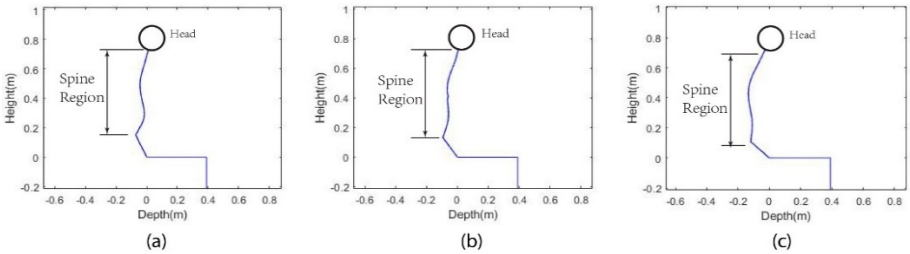

Fig. 2. Plot of the spine curve. (a) Erected posture, (b) Normal posture, (c) Slouched posture

Table 1. Joint angles for different postures

Posture	θ_1 (°)	θ_2 (°)	θ_3 (°)	θ_4 (°)	θ_5 (°)	θ_6 (°)	θ_7 (°)	θ_8 (°)
Erected	0	90	-64.6	-41.6	26.1	-19.7	-4.73	0.1
Normal	0	90	-54.4	-46.45	13.9	-18.3	-0.8	0.46
Slouched	0	90	-52.1	-47.6	5.1	-25.4	-5.8	0.1

Fig. 3 plots the spine model by including the backrest model. It indicates that for the erected and normal posture, initially both thoracic-1 and lumbar have a contact with the backrest simultaneously, but thoracic-2 is at a small distance away from the backrest. Therefore, it is reasonable to consider the initial contact with the backrest through thoracic 1 and lumbar and then progressing to thoracic-2. For the slouched posture, only thoracic-2 and lumbar would be in contact with the backrest. This is a posture that most likely to happen when a person sits up and leans forward for activities like reading and writing. It is quite unnatural for someone to have a slouched posture when leans back to relax. Therefore, the interaction between the human body and the backrest for the slouched posture is excluded.

For the other two postures, the points of initial contact can be estimated using Fig. 3. For the erected posture, it is approximately at 70% and 30% of the base line from the bottom for thoracic 1 and lumbar, respectively. For the normal posture, it is approximately at 50% and 50% of the base line from the bottom for thoracic 1 and lumbar, respectively.

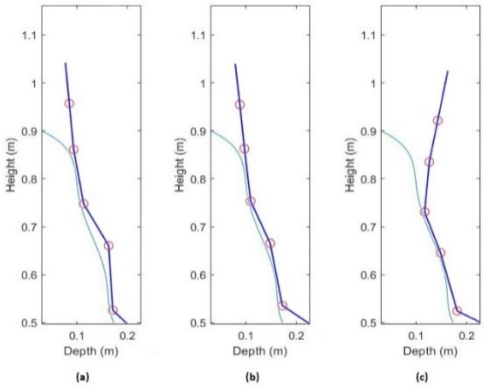

Fig. 3. Plot of segmented spine model against the mid cross-sectional profile of the backrest. (a) Erected posture, (b) Normal posture, (c) Slouched posture

2.3 Modeling of Contact Force

In this section, a multi-body dynamics method is applied to determine the body forces. starting with the segmented spine, which can be represented by links connected by revolve joints. In line with a backward recursive method [16], the forces and moments acting on the *i*th joint can be expressed from the head through the spine segments to the pelvis as

$$\mathbf{w}_i = \mathbf{M}_i \dot{\boldsymbol{t}}_i^J + \mathbf{B}_i + \mathbf{H}_{ii+1}\mathbf{w}_{i+1} + \mathbf{N}_{ii+1}\boldsymbol{w}_{ni} \tag{5}$$

where $\mathbf{w}_\mathrm{i} = [\mathbf{f}_\mathrm{i} \quad \mathbf{m}_\mathrm{i}]^\mathbf{T}$ is the wrench consisting force vector$\mathbf{f}_\mathrm{i}$ and moment vector $\mathbf{m}_\mathrm{i}$ of the *i*th joint, $\mathbf{M}_i = \begin{bmatrix} m_i \boldsymbol{E}_{3\times3} & m_i \tilde{\mathbf{b}}_{Ci}^{S\,T} \\ m_i \tilde{\mathbf{b}}_{Ci}^{S} & \mathbf{I}_i \end{bmatrix}$ is the generalized mass matrix of the *i*th segment, m_i is the segment mass, $\boldsymbol{E}_{3\times3}$ is the unitary matrix, $\tilde{\mathbf{b}}_{Ci}^{S}$ is the skew matrix of centroid vector, $\mathbf{b}_{Ci}^{S}$, $\dot{\boldsymbol{t}}_i^J = \begin{bmatrix} \mathbf{a}_i - \mathbf{g} \\ \boldsymbol{\alpha}_i \end{bmatrix}$ is called twist including linear acceleration vector $\mathbf{a}_i - \mathbf{g}$ and angular acceleration vector $\boldsymbol{\alpha}_i$, vector $\mathbf{B}_i = \begin{bmatrix} m_i \boldsymbol{\omega}_i \times (\boldsymbol{\omega}_i \times \tilde{\mathbf{b}}_{Ci}^{S}) \\ \boldsymbol{\omega}_i \times (\mathbf{I}_i \boldsymbol{\omega}_i) \end{bmatrix}$ is the matrix includes centrifugal forces and gyroscopic moments, $\mathbf{w}_{i+1}$ is the wrench for the upper (*i*+1)th joint, $\mathbf{H}_{ii+1} = \begin{bmatrix} \boldsymbol{E}_{3\times3} & \mathbf{0} \\ \tilde{\mathbf{b}}_i^S & \boldsymbol{E}_{3\times3} \end{bmatrix}$ is the transformation matrix between two adjacent joints, and $\mathbf{b}_i^S$ is the vector from the *i*th joint to (*i*+1)th joint, $\mathbf{N}_{ii+1} = \begin{bmatrix} \mathbf{0} & \mathbf{0} \\ \tilde{\mathbf{b}}_{ni}^S & \mathbf{0} \end{bmatrix}$is the transformation matrix of the contact wrench $\boldsymbol{w}_{ni}$ and $\mathbf{b}_{ni}^S$ is the vector from the *i*th joint to the contact point of the *i*th segment.

For quasi-static case that represents the normal human sitting in the seat, it is reasonable to assume negligible velocity and acceleration, i.e. $\boldsymbol{\omega}_i = 0$, then $\mathbf{B}_i = 0$ and $\dot{\boldsymbol{t}}_i^J = [-\mathbf{g} \quad \mathbf{0}]^T$ Projecting $\boldsymbol{w}_i$ about the rotation z-axis leads to the moment equilibrium equation as

$$\tau_i = \boldsymbol{z}_i \cdot \mathbf{m}_i^T = 0 \tag{6}$$

Substituting the moment vector into Eq. (6) yields

$$0 = \boldsymbol{z}_i \cdot \left(-m_i \tilde{\mathbf{b}}_{Ci}^S \mathbf{g} + \tilde{\mathbf{b}}_i^S \boldsymbol{f}_{i+1}^T + \tilde{\mathbf{b}}_{ni}^S \boldsymbol{f}_{ni}^T\right) \tag{7}$$

For a planar case, the above model can be greatly simplified to determine the normal contact force of the *i*th segment as

$$f_{ni} = \frac{(f_{i+1} b_i \sin(\theta_{i+1}) + m_i g b_{Ci} \sin(\delta_i))}{b_{ni}} \tag{8}$$

where $f_{ni} = \|\boldsymbol{f}_{ni}\|$, $b_i = \|\mathbf{b}_i^S\|$,, $g = \|\mathbf{g}\|$, $b_{Ci} = \|\mathbf{b}_{Ci}^S\|$, $b_{ni} = \|\mathbf{b}_{ni}^S\|$,, δ_i is the intersection angle between the gravity vector and the segment line vector $\overrightarrow{o_i o_{i+1}}$, expressed as

$$\delta_i = \cos^{-1}\left(\frac{\overrightarrow{o_i o_{i+1}} \cdot m_i \mathbf{g}}{\|o_i o_{i+1}\| \|m_i \mathbf{g}\|}\right) \tag{9}$$

Then, the tangential force can be expressed as

$$f_{ti} = m_i g \cos(\delta_i) + f_{i+1} \cos(\theta_{i+1}) \tag{10}$$

The friction force can be determined as

$$f_{fi} = f_{ni} u \tag{11}$$

where u is the friction coefficient. In terms of the forces passing down from the upper segment to the lower segment, there are two cases. The first case is no contact in that segment $\boldsymbol{w}_{ni} = 0$, then the segment weight will be completely passed down to the next segment. The second case is with contact $\boldsymbol{w}_{ni} \neq 0$, the force in the normal direction will be balanced, but the tangential force will be passed down to the next joint as

$$f_{di} = \begin{cases} 0 & i = 9 \\ f_{ti} + f_{ni} u & i < 9 \end{cases} \tag{12}$$

where i=9 indicates the head. As an example, the force from the head to the neck is described below. Referring to Fig. 4, the normal force, tangential force and friction force on the head can be expressed as:

$$f_{n8} = \frac{(m_8 g b_{C8} \sin(\delta_8))}{b_{n8}} \tag{13}$$

$$f_{t8} = m_8 g \cos(\delta_8) \tag{14}$$

$$f_{f8} = f_{n8} u \tag{15}$$

where $\delta_8 = \cos^{-1}\left(\frac{\overrightarrow{o_8 o_9} \cdot m_8 \mathbf{g}}{\|o_8 o_9\| \|m_8 \mathbf{g}\|}\right)$. The total force from the head passed to the neck is

$$f_{d8} = m_8 g \cos(\delta_8) + \frac{(0 + m_8 g b_{C8} \sin(\delta_8))}{b_{n8}} u \tag{16}$$

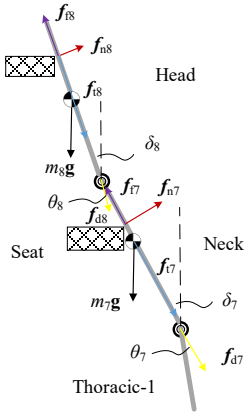

Fig. 4. Case for head and neck

For the neck, the normal force is

$$f_{n7} = \frac{(f_{d8} b_7 \sin(\theta_8) + m_7 g b_{C7} \sin(\delta_7))}{b_{n7}} \tag{17}$$

and

$$\delta_7 = \cos^{-1}\left(\frac{\overrightarrow{o_7o_8}\cdot m_7\mathbf{g}}{\|o_7o_8\|\|m_7\mathbf{g}\|}\right) \tag{18}$$

The tangential force and friction force are

$$f_{t7} = m_7 g\cos(\delta_7) + f_{d8}\cos(\theta_8) \tag{19}$$

$$f_{f7} = f_{n7}u \tag{20}$$

The total force passed down to the next segment is

$$f_{d7} = f_{t7} + f_{f7} = f_{t7} + f_{n7}u \tag{21}$$

Note from Eq (13), (17) that if $b_{ni} = 0$ i.e. the point of contact is neat the joint, f_{ni} become infinite. When this happens, an easy way to solve this problem is to further segment the spine so that the point of contact does not get closer to the joint.

2.4 Modeling of Contact Stress

For contact stress analysis, the normal force is used. Since the average human body is concave in the middle along the spine, f_{ni} is divided by 2 (or in more general case, see Eq (32) later in the paper) and placed at bi-lateral locations according to the body shape. For the segment of thoracic 1 the forces are placed on the midpoint of the scapula at the vertical position corresponding to the initial contact. For segments of thoracic 2 and lumbar, the forces are placed at the midpoints of the muscle group erector spinae. While the normal does change at different locations compared to the center of the body, the effect is small.

With the force determined, the pressure distribution can be calculated using the contact mechanics [17-19]. The contact area between two contact bodies forms an ellipse. The maximum stress, located at the initial contact point, can be related to the semi-minor axis of the ellipse with

$$P_0 = \frac{b}{E(k')\Delta} \tag{22}$$

where $E(k') = \int_0^{\frac{\pi}{2}}\sqrt{1-k'^2\sin^2\theta}\,d\theta$ is a complete elliptic integral of the second kind, $\Delta = \frac{1}{A+B}\left(\frac{1-\nu_1^2}{E_1}+\frac{1-\nu_2^2}{E_2}\right)$, $k = \frac{b}{a}$, $k' = \sqrt{1-k^2}$. E_is are the Young's modulus of the contacting bodies and ν_is are their passion ratio. A and B are functions of geometrical properties that largely depend on the principle radiuses of the two contacting bodies, i.e. seat and the human body. k can be determined by solving the equation below numerically as

$$\frac{B}{A} = \frac{\frac{1}{k^2}E(k') - K(k')}{K(k') - E(k')} \tag{24}$$

The stress distribution follows

$$P(x,y) = P_0\left(1 - \left(\frac{x}{a}\right)^2 - \left(\frac{y}{b}\right)^2\right)^{1/2} \tag{25}$$

The applied force is given by

$$F = \frac{2\pi E^2(k')\Delta^2 P_0^3}{3k} = \frac{2\pi b^3}{3kE(k')\Delta} \tag{26}$$

The values of the semi-major axis of the contact area a can be determined with

$$a = \sqrt[3]{\frac{3E(k')}{2\pi k^2}(F\Delta)} \tag{27}$$

Combining this contact stress theory with the force analysis, the applied force in Eq (26) is equal to the normal forces in Eq (8). In order to determine maximum stress with Eq (26), the geometrical data and material properties of the contacting bodies are needed. Starting with the geometrical data, the

cabin seat shape is measured to obtain the surface function $f(x,y)$ with curve fitting method. Once this is known, the principle radii can be calculated using the theory of differential geometry [20]. As for the human body, the principle radius in the vertical direction roughly follows the instantaneous radius of the spine which can be easily calculated using Eq (1-3). The principle radius in the horizontal direction can vary greatly based on body type. Strictly speaking, the principle radii of the human body do not follow the vertical or horizontal direction, and their directions change from head to toe. However, making them along the vertical and horizontal direction is a good approximation.

As for the material properties, both seat cushion and the human muscle are hyperelastic material. In this study, the Ogden hyperelastic material is used for cushion, and the ballistic gel is used to simulated the material properties of the human body. The stress-strain curve for both materials were experimentally obtained [21,22] and curve fit to obtain a polynomial equation. Differentiating the stress-strain equation yields $E(\varepsilon)$, i.e. Young's modulus as a function of strain ε. Then, from the original stress-strain data and the function $E(\varepsilon)$, a series of Young's modulus and stress pairs is obtained corresponding to the same strain. There pairs are then curve fitted to obtain $E(\sigma)$ or $E(P)$. The resulting equations are

$$E_s = 2.958\times10^{-12}x^4 - 1.549\times10^{-7}x^3 + 0.002783x^2 - 8.344x + 65490 \quad (28)$$

$$E_H = 6.383\times10^{-12}x^4 - 2.868\times10^{-7}x^3 + 0.004635x^2 - 8.545x + 40330 \quad (29)$$

where E_s is the Young's modulus for the seat cushion and E_H is the Young's modulus for the human body. As for Poisson ratio, the archived research shows that for the cushion, this ratio is close to 0, while for the human body, it is close to 0.5.

Now Eq (26) can now be written as

$$\left(\left(\frac{1-\nu_s^2}{E_s(P_0)}+\frac{1-\nu_H^2}{E_H(P_0)}\right)\right)^2 P_0^3 = \frac{3k(A+B)^2F_{ni}}{2\pi E^2(k')} \quad (30)$$

This can be easily solved numerically for P_0. At the end, the semi-major and semi-minor axis of the contact ellipse can be determined using Eq (26), (27), and the pressure distribution can be plotted with Eq (25). To validate the result, the normal force can be calculated with

$$F_n = \int P(x,y)da \quad (31)$$

and to compare with the normal force calculated with Eq (8)

3 Simulation and Analysis

Based on the methods described above, a simulation system has been developed as shown in the flow chart in Fig. 5. The side sitting position is for when people leaning on one side of their body. When this happens, f_{ni} cannot be simply divided by 2. The left-side normal force f_{ni}^L, and the right-side normal force f_{ni}^R should be calculated with

$$f_{ni}^L = af_{ni},\ f_{ni}^R = (1-a)f_{ni} \quad (32)$$

a depends on the angle of the tilt.

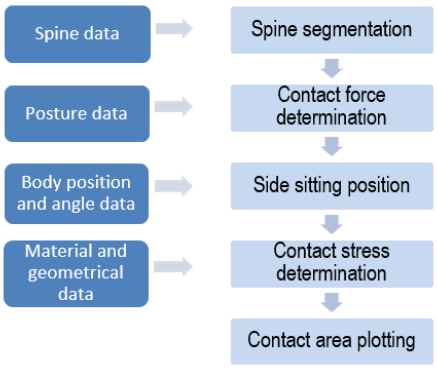

Fig. 5. Simulation flow chart

An average sized athletic human male is selected for simulation with the measurement: 175cm tall, 32-inch waist, 44-inch chest, 85Kg, muscular build, sitting in the seat with 135 degree recline angle. The simulated pressure distribution is plotted in Fig. 6. For the following plots, Fig. (6), (7), (8b), the height axis covers the spine from the neck to the pelvis. In more detail, 0 to 0.08 is pelvis region (partial), 0,08-0.2 lumbar, 0.2-0.35 thoracic-2, 0.35-0.47 thoracic-1, 0.47-0.5 cervical (partial). The entire height axis, 0-0.5, is the range of the backrest.

Fig. 6 shows that the pressure distribution looks similar for both postures in the upper spine, but the lower spine differs. The reason is that the erected posture has the arched-up profile in the lower spine region as shown in Fig. 3.

Fig. 7 shows the pressure distribution with two different backrest recline angles. The pressure of the higher spine region differs, and increases with the recline angle. However, the pressure remains similar in the lower spine region. The reason for this is that the normal force that the body exerted on the backrest, and therefore the pressure distribution is affected by two factors. One is the recline angle, and the other is the force that higher segments applied onto the lower segments, refers to Eq (16). For higher segments of the upper body, the force applied downwards onto them is either low or none. Also, this downward force effect is affected by the joint angle as seen in Eq (8), (17), which are near 0 or small as seen in table (1). This makes the first term in Eq (8), (17) negligible. Therefore, the pressure distribution between the higher segments of the upper body and the backrest is mostly affected by the recline angle as seen in Eq (13). As for the lower segments of the upper body, not only the force applied downwards onto them is higher, but also the joint angle is larger as seen in table (1). This can cause the downward force from the upper segments contribute significantly to the normal force that the lower segments of the upper body applied on the backrest. However, also seen in Eq (16) this downward force reduces as the recline angle increase, since most of the higher segments' weight is supported by the backrest instead of passing down at high recline angle. Because of this, for the lower segments of the upper body, the first term of the Eq (8) decrease while the second term increase as the recline angle increase, and vice visa. This can result the pressure in the lower spine region remain relative constant as the recline angle changes.

Fig. 8 shows the comparison between sensor data and simulation. The pressure sensors developed measures the pressure under the lumbar area. The simulated case is for side sitting, i.e. the human tilts on one side. It can be seen that the trend matches though the actual value differs, perhaps due to inaccurate calibration. In simulation, the force parameters are adjusted according to the tilt (with a in the Eq (32) set to be 0.3) and plotted in Fig. (8b). Comparing the sensor data with the simulation in 0.08 to 0.2 region on the height axis, highlighted in the white box, the simulation shows a similar shape and contrast. This gives some validation to the model.

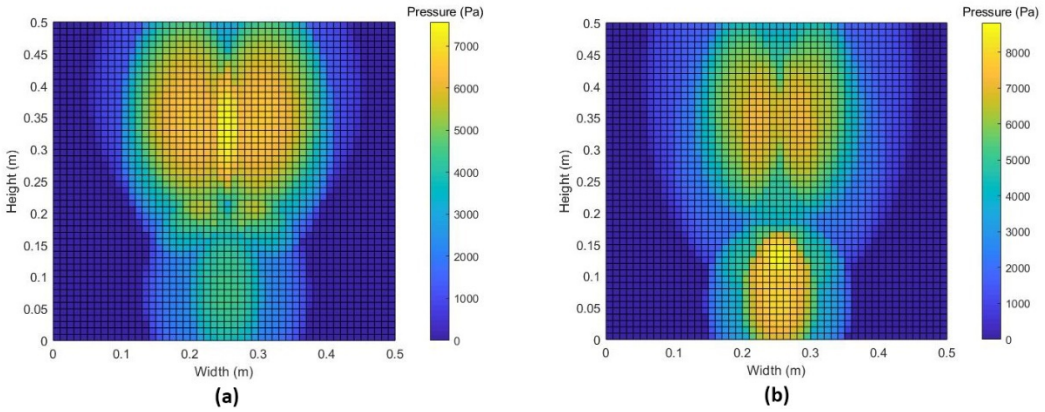

Fig. 6. Plot of pressure distribution. (a) Normal postural, (b) Erected posture.

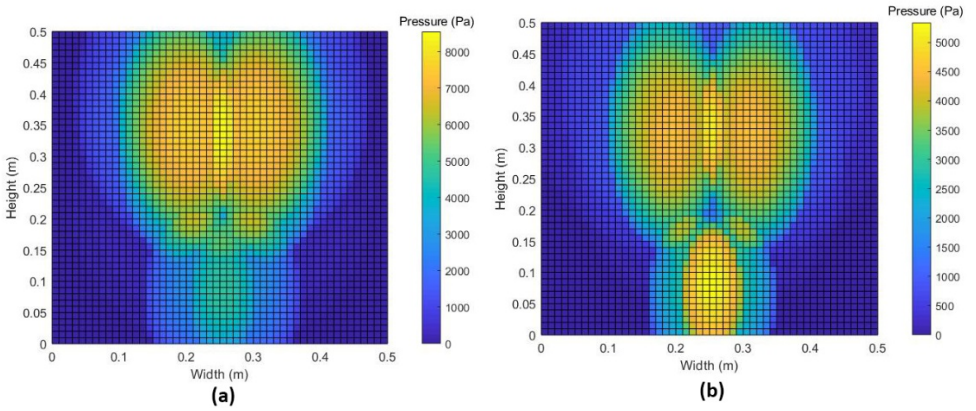

Fig. 7. Plot of pressure distribution (a) 150 degree recline, (b) 120 degree recline

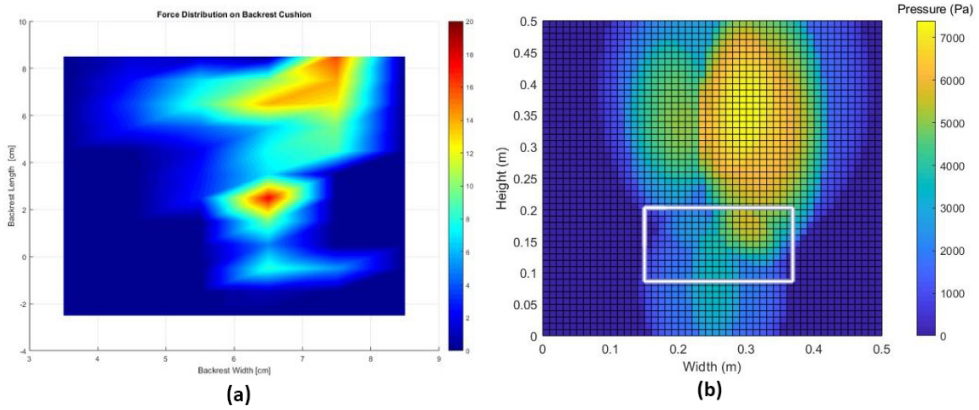

Fig. 8. Plot of pressure distribution. (a) Sensor data of the lumbar area, (b) simulation

4 Conclusion

A method for modeling the interaction between human body and aircraft seat for the comfortability analysis is presented in this paper. The method consists the modelling and force analysis of the human body with bio mechanics, geometrical and material analysis of the cabin seat and human body, and the pressure distribution analysis using contact stress theory. The simulation results show that different spine posture can affect the resulting pressure distribution. Also, when the recline angle changes, its

effect on the pressure distribution mostly occurs at the upper body, while the lower body has less effect. The simulation is compared with the sensor measurement to provide a validation to this method.

References

[1] Cohen D. An objective measure of seat comfort. Aviation Space & Environmental Medicine, 1998, 69(4):410.

[2] Christophy M, Senan N A F, Lotz J C, et al. A Musculoskeletal model for the lumbar spine. Biomechanics and Modeling in Mechanobiology, 2012, 11(1-2):19-34.

[3] Yue Y, Yun L, Bo P. Analysis and assessment of the seat geometry comfort for public passenger vehicles. 2011 International Conference on Electric Information and Control Engineering, 2011, Wuhan, China

[4] Huo X, Sun W L, Tao Q, et al. Seat comfort test and evaluation based on sitting posture analyses. Chinese Journal of Engineering Design, 2017.

[5] Matsushita Y ,Kuwahara N , Morimoto K . Relationship between Comfortable Feelings and Distribution of Seat Pressure in Sustaining a Sitting Posture for a Long Time// International Conference on Human-computer Interaction. Springer International Publishing, 2014.

[6] Reynolds, Mac. Sitting posture in design position of automotive interiors. International Journal of Human Factors Modelling and Simulation, 2012, 3(3/4):276.

[7] Aissaoui R , Lacoste M , Dansereau J . Analysis of sliding and pressure distribution during a repositioning of persons in a simulator chair. IEEE Transactions on Neural Systems and Rehabilitation Engineering, 2001, 9(2):215-224.

[8] Na S , Lim S , Choi H S , et al. Evaluation of driver's discomfort and postural change using dynamic body pressure distribution. International Journal of Industrial Ergonomics, 2005, 35(12):1085-1096.

[9] De Looze M P, Kuijt-Evers L F M, Van DieeN J. Sitting comfort and discomfort and the relationships with objective measures. Ergonomics, 2003, 46(10):985-997.

[10] Min Z. Experimental study on temperature sensation and pressure distribution of sitting posture. Nanjing Forestry University, 2007.

[11] Ciaccia F R D A S, Sznelwar L I . An approach to aircraft seat comfort using interface pressure mapping.. Work, 2012, 41 Suppl 1(6):240.

[12] Grujicic M, Pandurangan B, Xie X, et al. Musculoskeletal computational analysis of the influence of car-seat design/adjustments on long-distance driving fatigue. International Journal of Industrial Ergonomics, 2010, 40(3):345-355.

[13] Gragg J., Yang J. (James), and Long J. D. Digital Human Model for Driver Seat Adjustment Range Determination. SAE Technical Paper Series.2010-01-0386.

[14] Rasmussen J, Tørholm S, Zee M D. Computational analysis of the influence of seat pan inclination and friction on muscle activity and spinal joint forces. International Journal of Industrial Ergonomics, 2009, 39(1):52-57.

[15] Kitazaki S, Griffin M J. A modal analysis of whole-body vertical vibration, using a finite element model of the human body. Journal of Sound and Vibration, 1997, 200(1): 83-103

[16] Xi, F. Computational Dynamics, Lecture Notes, Ryerson University

[17] Rososhansky M, Xi F, and Li Y; Coverage Based Tool Path Planning for Automated Polishing Using Contact Stress Theory; 2010 IEEE International Conference on Automation Science and Engineering, 2010

[18] Liao L and Xi F, A Linearized Model for Control of Automated Polishing Process, in Proceeding of 2005 IEEE Conference on Control Applications, Toronto, Canada, August 28-31, 2005.

[19] A.P. Boresi, R.J. Schmidt, O.M. Sidebottom, Advanced mechanics of materials, Fifth ed., Wiley, 1993.

[20] Thomas Banchoff, Stephen Lovett; Differential Geometry of Curves and Surfaces; CRC Press, Taylor & Francis Group, LLC, 2010

[21] Campos, G, Xi F. Pressure sensing and control of an aircraft passenger seat, 1st ICC, 2016.

[22] Martins P. A. L. S, Natal Jorge R. M, Ferreira A. J. M; A Comparative Study of Several Material Models for Prediction of Hyperelastic Properties: Application to Silicone-Rubber and Soft Tissues; Strain 42(3):135-147, August 2006